ResearchGate

See discussions, stats, and author profiles for this publication at: https://www.researchgate.net/publication/261105570

Thiazole-Based γ-Building Blocks as Reverse-Turn Mimetic to Design a Gramicidin S Analogue: Conformational and Biological Evaluation

ARTICLE *in* CHEMISTRY - A EUROPEAN JOURNAL · MAY 2014

Impact Factor: 5.73 · DOI: 10.1002/chem.201402190 · Source: PubMed

CITATIONS
5

READS
68

10 AUTHORS, INCLUDING:

Vincent Lisowski
Université de Montpellier
56 PUBLICATIONS **900** CITATIONS
SEE PROFILE

Nicolas Masurier
Université de Montpellier
28 PUBLICATIONS **196** CITATIONS
SEE PROFILE

Séverine Zirah
Muséum National d'Histoire Naturelle
44 PUBLICATIONS **1,228** CITATIONS
SEE PROFILE

Jean Martinez
Université de Montpellier
960 PUBLICATIONS **12,419** CITATIONS
SEE PROFILE

Available from: Nicolas Masurier
Retrieved on: 24 January 2016

ChemPubSoc Europe

DOI: 10.1002/chem.201402190

CHEMISTRY
A European Journal
Full Paper

Amino Acids

Thiazole-Based γ-Building Blocks as Reverse-Turn Mimetic to Design a Gramicidin S Analogue: Conformational and Biological Evaluation

Baptiste Legrand,[a] Loïc Mathieu,[a] Aurélien Lebrun,[a] Soahary Andriamanarivo,[a] Vincent Lisowski,[a] Nicolas Masurier,[a] Séverine Zirah,[b] Young Kee Kang,[c] Jean Martinez,[a] and Ludovic T. Maillard*[a]

Abstract: This paper describes the ability of a new class of heterocyclic γ-amino acids named ATCs (4-amino(methyl)-1,3-thiazole-5-carboxylic acids) to induce turns when included in a tetrapeptide template. Both hybrid Ac-Val-(*R* or *S*)-ATC-Ile-Ala-NH_2 sequences were synthesized and their conformations were studied by circular dichroism, NMR spectroscopy, MD simulations, and DFT calculations. It was demonstrated that the ATCs induced highly stable C_9 pseudocycles in both compounds promoting a twist turn and a reverse turn conformation depending on their absolute configurations. As a proof of concept, a bioactive analogue of gramicidin S was successfully designed using an ATC building block as a turn inducer. The NMR solution structure of the analogue adopted an antiparallel β-pleated sheet conformation similar to that of the natural compound. The hybrid α,γ-cyclopeptide exhibited significant reduced haemotoxicity compared to gramicidin S, while maintaining strong antibacterial activity.

Introduction

Among the various secondary structures, reverse turns are one of the major structural elements in biologically active peptides and globular proteins. They are key features for protein folding by pre-organizing polypeptide chains and are involved in many of the molecular recognition events in biological systems.[1] They are also an essential part of antimicrobial peptides that contain β-hairpins or β-sheets, for example, protegrin, tachyplesin, defensins and gramicidin S.[2] In this context, numerous efforts have been made to develop small-turn inducers. A large variety of scaffolds derived from β-amino acids have been characterized,[3] while homo- or heterogeneous sequences incorporating γ-amino acids have received far less attention due, in part, to the difficulty to access stereochemically pure γ-building blocks.[3e,f,4] Mann and Kessler reported the first example of (hetero)aromatic-based γ-amino acids in which the ring is an oxazole. They suggested that when included into a small peptide, such a γ-amino acid building block induced a C_9 turn.[4d] However, the turn conformation was not fully characterized.

We recently described a new class of constrained heterocyclic γ-amino acids built around a thiazole ring, that is, 4-amino-(methyl)-1,3-thiazole-5-carboxylic acids (ATCs, **1a** and **2**; Figure 1). We demonstrated the high propensity of ATC oligomers to adopt a C_9 helical structure in solid and solution states in both organic solvents and water.[5] We now report the synthesis of α-α-ATC-α hybrid tetrapeptides and their structural studies by circular dichroism (CD), NMR spectroscopy, molecular dynamic simulations, and DFT calculations. To investigate the impact of the ATC configuration on the peptide shape, we prepared the two diastereomers **3a** and **3b** consisting in Ac-Val-(*S* or *R*)ATC-Ile-Ala-NH_2 (Figure 1). Based on our structural data, the (*R*)-ATC motif was then selected as a surrogate for the D-Phe-Pro turn to synthesize a biologically active analogue of the gramicidin S (GS; Figure 1), a highly haemolytic β-hairpin cyclodecapeptide antibiotic. The antimicrobial and haemolytic activities of analogue **4** (Figure 1) were tested and its NMR solution structure was determined and compared to the characteristic β-pleated sheet of the GS.

[a] *Dr. B. Legrand,[+] L. Mathieu,[+] A. Lebrun, S. Andriamanarivo, Prof. V. Lisowski, Dr. N. Masurier, Prof. J. Martinez, Dr. L. T. Maillard*
Institut des Biomolécules Max Mousseron
UMR 5247, CNRS, Universités Montpellier I et II
UFR des Sciences Pharmaceutiques et Biologiques
15 Avenue Charles Flahault, 34093 Montpellier Cedex 5 (France)
Fax: (+33) 4-67-54-86-54
E-mail: ludovic.maillard@univ-montp1.fr

[b] *Dr. S. Zirah*
Muséum National d'Histoire Naturelle (MNHN)
UMR 7245 CNRS/MNHN
Molécules de Communication et Adaptation des Micro-organismes (MCAM)
57, rue Cuvier, 75005 Paris (France)

[c] *Prof. Y. K. Kang*
Department of Chemistry and BK21 PLUS Research Team
Chungbuk National University
Cheongju, Chungbuk 361-763 (Republic of Korea)

[+] *These authors contributed equally to this work.*

Supporting information for this article is available on the WWW under http://dx.doi.org/10.1002/chem.201402190.

© 2014 Wiley-VCH Verlag GmbH & Co. KGaA, Weinheim

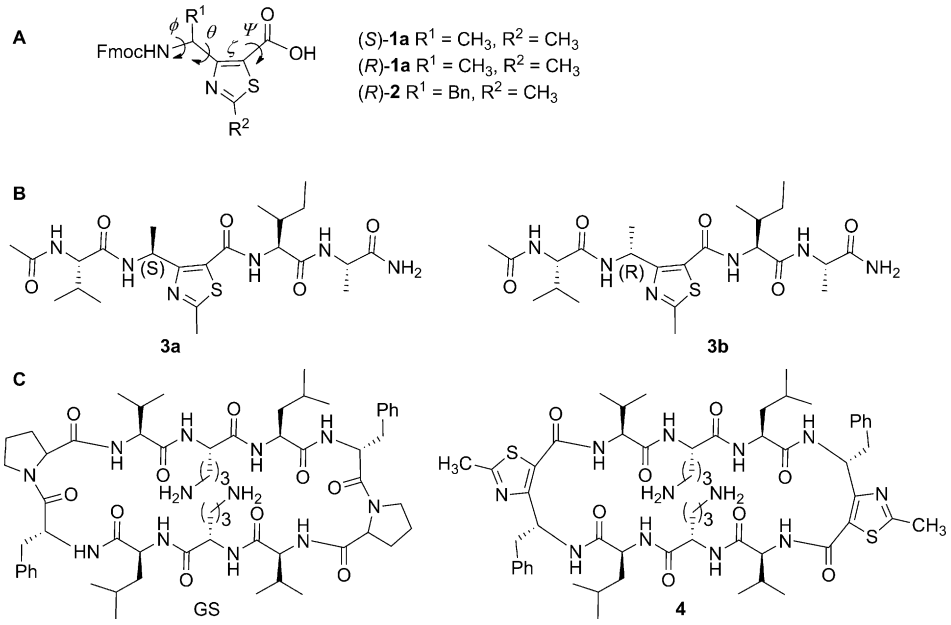

Figure 1. Structures of A) the ATC building blocks, B) of the α-α-(*R or S*)-ATC-α hybrid tetrapeptides **3a** and **3b** and C) of gramicidin S (GS) and ATC-based gramicidin S analogue **4**.

Results and Discussion

Syntheses and NMR studies of hybrid tetrapeptides 3a and 3b

Peptides **3a** and **3b** were synthesized by solid-phase peptide techniques on rink amide resin starting from ATC building blocks (*S* or *R*)-**1a** using the Fmoc strategy (Fmoc = 9-fluorenylmethoxycarbonyl). NMR spectra of peptides **3a** and **3b** (5 mM) were recorded in CD_3OH and [D_6]DMSO at 298 K. Whatever the solvent considered, protons resonances of the C-terminal moiety (Ile-Ala) of **3a** and **3b** were remarkably similar ($\Delta\delta_H <$ 0.05 ppm), while significant variations were observed for the Ile-HN, ATC-HN, ATC-Hγ protons and the Val resonances, suggesting the ATC-C_γ configuration mainly affected the conformation of the N-terminal part. The amide proton signals that followed the ATCs (i.e., Ile) in **3a** and **3b** were strongly shifted downfield at 9.72 and 9.94 ppm, respectively, in CD_3OH (9.32 and 9.30 ppm, respectively, in [D_6]DMSO) and both peptides exhibited characteristic strong ROE correlations (ROE = rotating frame Overhauser effect) between Ile-HN and ATC-Hγ. Interestingly, such unshielded amide resonances along with strong HN(*i*+1), Hγ(*i*) correlations were typical of the poly-ATC 9-helix, supporting the presence of a (Ile)NH···OC(Val) hydrogen bond forming a C_9 pseudocycle. Moreover, the CD spectra of **3a** and **3b** in methanol exhibited quasi-symmetric signatures very close to those previously reported for a (*S,S*)-ATC dimer, which displayed a typical C_9 turn.[5] Such a nine-membered ring was fully characterized in the crystal structure and NMR spectra of the poly-ATC compounds.[5]

Hydrogen bonding was evaluated by DMSO-titration experiments with gradual addition of [D_6]DMSO to a solution of **3a** and **3b** in $CDCl_3$ (Figure S1 B in the Supporting Information) and by measuring the temperature coefficients of amide proton resonances in [D_6]DMSO between 293 and 333 K (Figures S2 and S3 in the Supporting Information). For **3a**, we could dissociate two groups of HN. While Ile, Ala-HN, and one proton of the NH_2 group exhibited small solvent chemical shifts dependency ($\Delta\delta < 0.9$ ppm), the other amide protons were accessible to the solvent according to their significant resonance variations upon [D_6]DMSO addition ($\Delta\delta > 1.4$ ppm). For **3b**, the solvent variations were globally less significant. We observed that the Ala- and Ile-HN resonances were less sensitive to [D_6]DMSO ($\Delta\delta <$ 0.6 ppm) than those of Val- and ATC-HN, supporting the idea that they might be hydrogen bonded. As formerly observed for the ATC oligomers, the HN resonances of both **3a** and **3b** were highly temperature dependent in [D_6]DMSO ($-4.0 \leq \Delta\delta/\Delta T \leq -4.6$ ppb K^{-1}, Table S8 in the Supporting Information), suggesting all the HN protons were exposed to the solvent. Nonetheless, temperature coefficient values could be highly influenced by deshielding effects from surrounding residues and/or by a partial temperature dependent loss of structure in small peptides.[6] The thiazole rings of the ATC backbone induced strong magnetic anisotropic effects, which highly influenced the neighboring proton chemical shifts (Ile-HN 9.72 and 9.94 ppm in CD_3OH) and prevented the interpretation of the variable-temperature experiments.

ROEs were used as constraints for the NMR structure calculations of **3a** and **3b** in CD_3OH using a typical simulated annealing protocol in vacuum with AMBER 11. Figure 2b shows a superimposition of the 20 lowest-energy structures of **3a** and **3b**. The two diastereomers exhibited well-defined structures stabilized by a C=O(*i*)···HN(*i*+2) hydrogen bond between the Ile-HN and the Val-CO, forming an ATC-residue-driven C_9 pseudocycle. Additionally, compound **3b** exhibited a subsequent hydrogen bond between the Ala-HN and the Val-CO to form a $C_{9/12}$ bidentate pseudocycle. The two peptides also displayed lateral hydrogen bonds, which formed C_{10} or C_7 pseudocycles on either side of the ATC residue. The torsion angle values of the ATC (Table S23 in the Supporting Information) were comparable to those measured in poly-(*S*)-ATC oligomers[5] ((*S*)-ATC in **3a**: $\phi = -54 \pm 2^\circ$, $\theta = 113 \pm 5^\circ$, $\zeta = -3 \pm 1^\circ$, $\psi = -14 \pm 3^\circ$; (*R*)-ATC in **3b**: $\phi = 57 \pm 2^\circ$, $\theta = -105 \pm 2^\circ$, $\zeta = 3 \pm 2^\circ$, $\psi = 10 \pm 2^\circ$; poly-(*S*)-ATC XRD structure: $\phi = -78 \pm 3^\circ$, $\theta = 127 \pm 14^\circ$, $\zeta = 0 \pm 3^\circ$, $\psi = -41 \pm 4^\circ$), while the orientation of the Val N-terminal residue was dependent of the configuration of the ATC-C_γ. Thus, (*S*)-ATC promoted a "twist"-turn conformation, while (*R*)-ATC induced a reverse turn like structure (Figure 2).

© 2014 Wiley-VCH Verlag GmbH & Co. KGaA, Weinheim

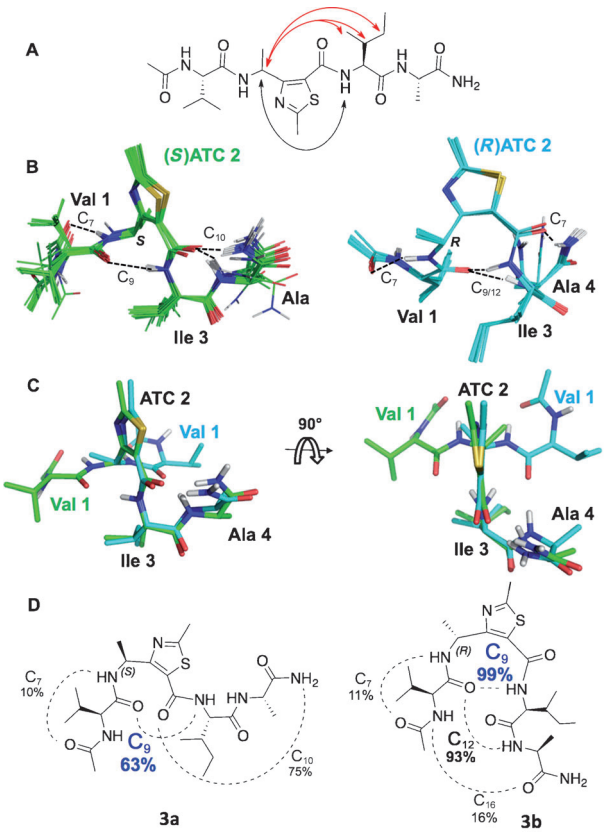

Figure 2. A) In black, typical NOE correlations stabilizing the C_9 pseudo cycle; in red, principal NOE correlations driving the folding. B) Overlay of the 20 lowest-energy structures of compounds **3a** (in green) and **3b** (in cyan). C) Superimposition of the NMR lowest energy structures of **3a** (in green) and **3b** (in cyan). D) Occurrence of the hydrogen bonding on **3a** (in green) and **3b** over 50 ns rMD (cutoff: $d_{O-N} < 3.5$ Å and N-H-O angle $> 120°$).

Molecular dynamic simulations

To get further insight on the stability of these structures and to investigate the set of conformations that **3a** and **3b** could adopt in solution, molecular dynamic simulations were achieved in a methanol box for 50 ns, starting from their lowest NMR structures. Simulations were launched using the inter-residue NOE-derived upper distances with (rMD) and without restraints (MD). The stability of each peptide folding during the simulations was assessed by computing: 1) the atom-positional root-mean-square deviation from the initial structure (RMSD); 2) the root-mean-square fluctuation (RMSF) values of the backbone heavy atoms (Figure S4 in the Supporting Information); 3) the occupancy of the hydrogen bonds along the simulations; and 4) the backbone dihedral angle distributions (Figure S5 in the Supporting Information).[7] The backbone RMSD were rather low over the restrained MD for both compounds (i.e., (0.43 ± 0.22) and (0.68 ± 0.22) Å for **3a** and **3b**, respectively) showing the two peptides conserved their overall conformations in methanol all along simulations. This was also reflected by the small RMSF values, which showed small oscillations on the central ATC and Ile residues, while the N and C termini (Val and Ala residues) underwent higher mobility for all trajectories. In both **3a** and **3b** the torsional angle distributions of the ATC residues were unimodal and narrow (Figure S5 in the Supporting Information). For the other residues, values were relatively low dispersed with minor populations, which explained the small variations of the RMSD. Only the ψ_1 dihedral angle distributions of Val were bimodal (Figure S5 in the Supporting Information), reflecting the larger fluctuation of the C-terminal atoms and explaining the small jumps on RMSDs (Figure S4 in the Supporting Information). The conformational behavior of **3a** and **3b** was studied by monitoring hydrogen-bond patterns over the simulations. With 63 and 75% occurrence, respectively, the C_9 pseudoring and the lateral C_{10} lateral pseudocycle in the "twist"-turn conformation **3a** imposed by (*S*)-ATC were moderately stable (Figure 2d, Table S22 in the Supporting Information). However, the $C_{9/12}$ hydrogen bonds stabilizing the reverse turn in **3b** induced by the (*R*)-ATC residue were more stable with a percentage of occupancy of 99 and 93%, respectively, during the 50 ns. The other hydrogen bonds were transients with a low occurrence < 16%.

During the unrestrained simulations, RMSFs were globally larger. The initial NMR conformation of **3b** was remarkably maintained (RMSD $= 0.61 \pm 0.17$ Å) during the 50 ns MD, confirming the high stability of the folding. The $C_{9/12}$ bidentate hydrogen bonds were preserved with 93 and 84% occupancy over the whole simulation. The most significant change occurred on the ψ_1 dihedral angle distribution of Val (Figure S5 in the Supporting Information) without impacting the peptide global shape. By comparison, after 1.5 ns, **3a** underwent a transition from a twist- to a reverse-turn structure stabilized by a bidentate $C_{9/12}$ pseudo cycle, mirroring the **3b** conformation. This structural rearrangement was associated with concomitant rotations of ψ_1, ϕ_2, and ϕ_3 dihedral angles (from 50 to $-7°$, -58 to $-112°$, and -59 to $-135°$, respectively), but was not compatible with NOE correlations observed between ATC-Hγ and Ile side chain protons. Although NMR spectroscopy could not ascertain the reverse-turn structure, since no characteristic NOEs could be found, the fast interconversion between the twist- and reverse-turn conformations in solution could not be excluded. Finally, in order to estimate the relative stabilities of the twist- and reverse-turn structures of **3a**, the MD structures were optimized at the B3LYP/6-31G(d) level of theory. The single-point energies of these two turn structures were calculated at the same level of theory with the conductor-like polarizable continuum model (CPCM)[8] in methanol. The twist-turn structure was found to be more stable by 3.40 kcal mol^{-1} than the reverse-turn structure in methanol, which indicates the relative populations of 99.7 and 0.3% for twist- and reverse-turn structures, respectively, at 298 K for **3a**.

DFT calculations

The stability of the C_9 and $C_{9/12}$ hydrogen bond(s) in **3a** and **3b** were also investigated by DFT calculations by using Gaussian 03.[9] The two lowest-energy NMR structures of **3a** and **3b** were optimized at the B3LYP/6-31G(d) level of theory. After optimization, both **3a** and **3b** displayed the C_9 hydrogen bond around the γ-amino acid. The C_{12} hydrogen bond suggested in **3b** by NOE data and MD simulations disappeared after optimi-

© 2014 Wiley-VCH Verlag GmbH & Co. KGaA, Weinheim

zation. As a consequence the C_9 C=O(*i*)···HN(*i*+2) hydrogen bond remained the major peptide folding driving force. The relative strength of the C_9 hydrogen bonds of the optimized structures was more deeply evaluated via the natural bond orbital (NBO) analysis[10] at the B3LYP/6-31+G(d,p) level of theory (Table 1). Compounds **3a** and **3b** shared similar values

Table 1. Relative strength of the hydrogen bonds calculated using the NBO method at the B3LYP/6-31+G(d,p)//B3LYP/6-31G(d) level of theory [units for atomic charges and Wiberg index in electrons, and the stabilization energies (ΔE_2) are in kcal mol^{-1}].

	Natural charges δ_O	δ_H	Wiberg index[a]	ΔE_2[b]
3a	−0.690	+0.465	0.705	16.17
3b	−0.690	+0.467	0.699	18.02

[a] Wiberg index indicates the strength of the Ile N–H bond. [b] The second perturbation energy of the lone pair orbitals of the oxygen with the corresponding N–H antibonding orbital, which is called the hyperconjugation is due to the charge transfer.[10]

of atomic charges and Wiberg index calculated for Ile N–H bond.[11] However, in accordance to rMD simulations, calculation of hyperconjugation (ΔE_2) term due to charge transfer showed that the C_9 hydrogen bond was more stable by about 2 kcal mol^{-1} in the reverse turn **3b** than in the "twist"-turn **3a**.

Synthesis and structural studies of the ATC-containing gramicidin S analogue 4

As a proof of concept, we present a successful application of the ATC C_9 turn for the design of a new derivative of the highly effective bactericidal gramicidin S (GS).[12,13] GS is an amphiphilic C_2-symmetrical cyclodecapeptide that adopts a highly stable antiparallel β-pleated sheet conformation stabilized by four intramolecular hydrogen bonds. The two strands are linked by two hydrophobic type II′ β-turns formed by D-Phe-Pro dipeptides. Detailed structure–activity relationship studies revealed that a large number of amino acid substitutions are tolerated,[13] while the stable, antiparallel β-sheet conformation is considered essential and is maintained among a wide range of derivatives.[14] Nevertheless, the major limitation in the clinical use of GS is due to its high lysogenic activity.[12] Considering (*R*)-ATC as a reverse-turn inducer, (*R*)-ATC **3c** was used as a surrogate for the D-Phe-Pro sequence to design the GS analogue **4**. The linear peptide was obtained by classical Fmoc solid-phase peptide synthesis then cyclized under high dilution conditions with HBTU/HOBt as a coupling reagent, purified by HPLC, and the side chains were deprotected (see the Supporting Information). GS was synthesized as a control under similar conditions. The NMR resonances of GS and the analogue **4** were fully assigned in [D$_6$]DMSO at 298 K. NMR observables (^3J(HNH$_\alpha$), amide proton temperature coefficients) for GS were similar to those previously reported (see Table S14–S19 in the Supporting Information). The entire set of ROE correlations was compatible with the XRD structure provided by Overhand and al.[15] A single set of signals was observed in **4** for the Val, Orn, Leu, and (*R*)-ATC suggesting that it also exhibited a C_2-symmetric structure. The amide protons following the ATC residue (i.e., Val HN) were strongly unshielded (9.28 ppm) as previously described for ATC oligomers and compounds **3a** and **3b**. The Val/Orn/Leu had relatively high ^3J(HNH$_\alpha$) coupling constants (8.0, 8.0, and 8.5 Hz, respectively) compatible with an extended conformation, but significantly lower than those of the GS. The corresponding ϕ torsional angles might display more degrees of freedom than in the natural GS. Temperature coefficients exhibited comparable trends than in GS, but with smaller values. The Orn and ATC-NH shared the higher values ($\Delta\delta/\Delta T = -3.8$ ppb K^{-1}) compared to the Val HN ($\Delta\delta/\Delta T = -2.5$ ppb K^{-1}) and Leu HN ($\Delta\delta/\Delta T = 0$ ppb K^{-1}). This suggested that these two first amide protons were solvent-shielded and involved in hydrogen bonding. Nevertheless, as previously discussed for **3a** and **3b**, the measured values for the amide protons close to the thiazole rings should be interpreted with caution. The typical strong ROE correlations between ATC-Hγ and the amide proton of the following residue (i.e., Val-HN) supported the presence of the ATC-driven C_9 pseudocycle. In addition, unambiguous long-range NOEs were observed between the Val and the Leu on either side of the C_9 turn (Table S19 in the Supporting Information). The solution structures of **4** were solved using 90 distances and 6 torsion angles restraints and exhibited a slightly distorted antiparallel β-pleated sheet stabilized by (*R*)-ATCs acting as reverse turns with C=O(*i*)···HN(*i*+2) hydrogen bonds (Figure 3a and b). As expected, the ATCs γ-amino acid adopted similar conformations in **3b** and **4** (Figure 3c). The dissymmetry of the C_9-turn of (*R*)-ATC may explain the non-ideal geometry of the sheet compared to that of the GS stabilized by the D-Phe-Pro dipeptide (C_{10}-turn). The major difference between **4** and GS arose from the flip of the benzyl

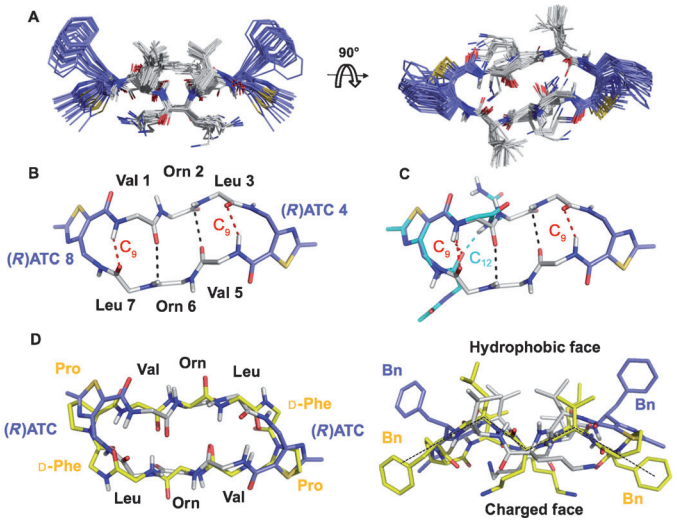

Figure 3. A) Overlay of the 20 lowest-energy NMR structures of **4** (ATC residues are in blue, protons are omitted for clarity). B) Backbone of the analogue **4**, hydrogen bonds are represented in dashed lines and C) superimposition of the backbone of **4** (white and blue for ATC) and the reverse-turn **3b** (cyan). D) Superimposition of the backbone of **4** (white and blue) and GS (yellow).

© 2014 Wiley-VCH Verlag GmbH & Co. KGaA, Weinheim

side chains from the charged face to the hydrophobic side of the sheet thus strengthening the amphipathicity (Figure 3d).

Antimicrobial activities

GS analogue **4** was then tested for its antimicrobial activity against a representative range of Gram-positive and Gram-negative bacteria strains. It conserved functional mimicry of the natural product although the antibiotic activities were slightly reduced. More importantly, the haemolytic activity of **4** was decreased sixfold (Table 2). Several studies support the haemotoxicity is highly correlated to the hydrophobicity and/or amphipathicity of the molecule.[16] As suggested by RP-HPLC analyses and by the re-orientation of the benzyl side chains, the haemotoxicity decrease could be explained in part by a higher hydrophilicity and amphiphilicity of **4** compared to GS.

Table 2. Antibacterial and haemolytic activities of **4** compared to GS.

	4	GS
E. coli[a]	25	12.5
Pseudomonas aeruginosa[a]	>50[b]	50[b]
S. aureus[a]	4.68	3.125
Bacillus subtilis[a]	3.125	1.56
hemolysis [%][c]	14	80

[a] Minimal inhibitory concentrations (MICs) in $\mu g\,mL^{-1}$ were determined after 48 h incubation. [b] 50 μM was the maximal tested concentration compatible with the compound solubility in culture media. [c] The percentage of haemolytic activity of red blood human cells caused at 100 μM peptide concentration.

Conclusion

We have demonstrated, using various techniques, that γ-amino acid ATC was able to induce a turn in solution when included in a short peptide sequence. It stabilized a typical C_9-turn with a similar geometry to that adopted in the 9-helix ATC oligomers. Depending on the configuration of the γ-amino acid stereocenter, ATCs could serve as turn mimetic. We successfully synthesized a gramicidin S analogue exhibiting reduced haemotoxicity, while maintaining interesting antibacterial activities. Considering the high diversity and the unique conformational properties of these γ-amino acid residues, we believe that the development of such turn mimics and their incorporation into biologically active molecules to constraint active conformations is of interest.

Experimental Section

General procedures

Commercially available reagents and solvents were used without any further purification. Reactions were monitored by HPLC using an analytical Chromolith Speed Rod RP-C18 185 Pm column (50× 4.6 mm, 5 μm) using a flow rate of $5.0\,mL\,min^{-1}$, and gradients from 100:0 to 0:100 eluents A/B over 3 min, in which eluents A = H_2O/TFA 0.1% and B = CH_3CN/TFA 0.1%. Detection was done at 214 and 254 nm using a photodiode array detector. Retention times are reported as follows: t_r (min). ^1H and ^{13}C NMR spectra were recorded at room temperature in deuterated solvents. Chemical shifts (δ) are given in parts per million relative to TMS or relative to the solvent (^1H: δ ($CDCl_3$) = 7.24 ppm; ^{13}C: δ ($CDCl_3$) = 77.2 ppm). The following abbreviations were used to designate the signal multiplicities: s (singlet), d (doublet), t (triplet), q (quartet), m (multiplet), br (broad). Analytical thin-layer chromatography (TLC) was performed using aluminium-backed silica gel plates coated with a 0.2 mm thickness of silica gel or with aluminium oxide 60 F254, neutral. LC-MS spectra (ESI) were recorded on an HPLC using an analytical Chromolith Speed Rod RP-C18 185 Pm column (50× 4.6 mm, 5 μm) using a flow rate of $3.0\,mL\,min^{-1}$, and gradients of 100:0 to 0:100 eluents A/B over 3 min, in which eluents A = H_2O/HCOOH 0.1% and B, CH_3CN/HCOOH 0.1%. High-resolution mass spectrometric analyses were performed with a time-of-flight (TOF) mass spectrometer fitted with an electrospray ionisation source (ESI). All measurements were performed in the positive ion mode. Melting points (m.p.) are uncorrected and were recorded on a capillary melting point apparatus. Enantiomeric excesses were determined by Chiral HPLC analysis using a Chiracel OD-R column (250 mm × 4.6 mm) with H_2O, TFA 0.1%/ACN, TFA 0.1%. (40: 60) as eluent and a flow rate of $1\,mL\,min^{-1}$.

Synthesis of (*S*)-1a, (*R*)-1b and 2

Compounds **1a**, **1b**, and **2** were synthesized from Fmoc-(*S*)-alanine, Fmoc-(*R*)-alanine and Fmoc-(*S*)-phenylalanine, according the previously described procedure.[5]

General procedure for the preparation of hybrid peptides 3a and 3b

Peptides **3a** and **3b** were synthesized by solid-phase methods using standard Fmoc chemistry. The peptides were assembled on ChemMatrix® Rink Amide resin loaded at $0.54\,mmol\,g^{-1}$. Chain elongations were performed with Fmoc-Ala-OH, Fmoc-Ile-OH, (*S*)-**1a** or (*R*)-**1b**, and Fmoc-Val-OH (0.3 mmol each), using 20% piperidine/NMP for Fmoc deprotection, HBTU/HOBt for activation (0.3 mmol each), *N*-methylmorpholine (NMM, 6 equiv) and NMP (5 mL) as solvent. After completion of the synthesis, the linear peptides were acetylated with Ac_2O/DCM (1:1 vv; 3×5 min), then cleaved from the resin with 100% CF_3COOH. After removing the solvent, the peptides were purified by preparative HPLC on a Delta Pak, C18 column (15 μm, 40×100 mm; Solvent A: H2O/TFA vol/vol 0.1%; Solvent B: MeCN/TFA vol/vol 0.1%; flow $20\,mL\,min^{-1}$; linear gradient A/B: from 85:15 to 60:40 in 30 min). HPLC analyses were performed on an analytical Chromolith Speed Rod RP-C18 185 Pm column (50×4.6 mm, 5 μm) using a flow rate of $5.0\,mL\,min^{-1}$, and gradients from 100:0 to 0:100 eluents A/B over 3 min, in which eluents A = H_2O/TFA 0.1% and B = CH_3CN/TFA 0.1%. Detections were done at 214 and 254 nm using a photodiode array detector. the retention times were determined to be 1.28 min for **3a** and 1.26 min for **3b**. Compounds **3a** and **3b** were obtained in 35 and 32% yields respectively. **3a:** t_r = 1.28 min; LC-MS: (ESI+): *m/z* (%): 511.2 (100) $[M+H]^+$, 533.2 (10) $[M+Na]^+$. **3b:** t_r = 1.26 min; LC-MS: (ESI+): *m/z* (%): 511.2 (100) $[M+H]^+$; for NMR data see Tables S1–S4 in the Supporting Information.

© 2014 Wiley-VCH Verlag GmbH & Co. KGaA, Weinheim

Synthesis of gramicidin S

The backbone-cyclic peptide was assembled on 2-chlorotrityl chloride resin (Novabiochem). Fmoc-Pro-OH (0.25 mmol) was loaded on 2-chlorotritylchloride resin (800 mg, loading 0.3 mmol g^{-1}) in the presence of *N*-methylmorpholine (NMM, 4 equiv) in CH_2Cl_2 (15 mL). The unreacted sites on the resin were capped by washing with a mixture of CH_2Cl_2/MeOH/DIPEA (17:2:1) followed by MeOH. Following removal of the Fmoc-group using 20% piperidine in *N*-methyl-2-pyrrolidinone (NMP), chain elongation was performed with Fmoc-D-Phe, Fmoc-Leu-OH, Fmoc-Orn(Boc)-OH, Fmoc-Val-OH, Fmoc-Pro-OH, Fmoc-D-Phe, Fmoc-Leu-OH, Fmoc-Orn(Boc)-OH, Fmoc-Val-OH (1 mmol each, 4 equiv), using 20% piperidine/NMP for Fmoc deprotection, HBTU (4 equiv) for activation, DIPEA as base and NMP as solvent. After completion of the synthesis, the linear peptide was cleaved from the resin with CF_3COOH/water (1:99 v/v). After removing the solvent, the peptide was cyclized overnight using HBTU (4 equiv) for activation, *N*-methylmorpholine (11 equiv) as base in DMF (30 mL). The solvent was removed under reduce pressure then the protected peptide was purified by preparative HPLC on a Delta Pak, C18 column (15 μm, 40×100 mm; Solvent A: H2O/TFA vol/vol 0.1%; Solvent B: MeCN/TFA vol/vol 0.1%; flow 20 mL min^{-1}; linear gradient A/B: from 50:50 to 10:90 in 30 min) and lyophilized. Boc removal was done using TFA/Water (9:1 v/v). Gramicidin S was recovered in 12% yield (39 mg). HPLC analysis was performed on an analytical chromolith speed rod RP-C18 185 Pm column (50×4.6 mm, 5 μm) using a flow rate of 5.0 mL min^{-1}, and gradient from 100:0 to 0:100 eluents A/B over 3 min, in which eluents A = H_2O/TFA 0.1% and B = CH_3CN/TFA 0.1%. Detections were done at 214 and 254 nm using a photodiode array detector. t_r = 2.14 min; LC-MS: (ESI+): *m/z* (%): 571.4 (100) $[M+2H]^{2+}$), 1141.8 (35) $[M+H]^+$; for NMR data see Tables S14 and S15 in the Supporting Information.

Synthesis of gramicidine S analogue 4

Compound **4** was synthesized according to the general procedure from Boc-β^3-hAla-OH (1.0 g, 4.99). The backbone-cyclic peptide was assembled on 2-chloro-trityl chloride resin (Novabiochem). Compound **2** (0.25 mmol) was loaded on 2-chloro-tritylchloride resin (800 mg, loading 0.3 mmol g^{-1}) in the presence of *N*-methylmorpholine (NMM, 4 equiv) in CH_2Cl_2 (15 mL). The unreacted sites on the resin were capped by washing with a mixture of CH_2Cl_2/MeOH/DIPEA (17:2:1) followed by MeOH. Following removal of the Fmoc-group using 20% piperidine in *N*-methyl-2-pyrrolidinone (NMP), chain elongation was performed with Fmoc-Leu-OH, Fmoc-Orn-(Boc)-OH, Fmoc-Val-OH, Fmoc-(*R*)-ATC **2**, Fmoc-Leu-OH, Fmoc-Orn-(Boc)-OH, Fmoc-Val-OH (1 mmol each, 4 equiv), using 20% piperidine/NMP for Fmoc deprotection, HBTU (4 equiv) for activation, DIPEA as base and NMP as solvent. After completion of the synthesis, the linear peptide was cleaved from the resin with CF3COOH/water (1:99 vv). After removing the solvent, the peptide was cyclized overnight using HBTU (4 equiv) for activation, *N*-methylmorpholine (11 equiv) as base in DMF (30 mL). The solvent was removed under reduced pressure then the protected peptide was purified by preparative HPLC on a Delta Pak, C18 column (15 μm, 40×100 mm; Solvent A: H_2O/TFA vol/vol 0.1%; Solvent B: MeCN/TFA vol/vol 0.1%; flow 20 mL min^{-1}; linear gradient A/B: from 50:50 to 10:90 in 30 min) and lyophilized. Boc removal was done using TFA/Water (9:1 v/v). The cyclopeptide **4** was recovered in 16% yield (45 mg). HPLC analysis was performed on an analytical chromolith speed rod RP-C18 185 Pm column (50×4.6 mm, 5 μm) using a flow rate of 5.0 mL min^{-1}, and gradients from 100:0 to 0:100 eluents A/B over 3 min, in which eluents A = H_2O/TFA 0.1% and B = CH_3CN/TFA 0.1%. Detections were done at 214 and 254 nm using a photodiode array detector. t_r = 1.78 min; LC-MS: (ESI+): *m/z* (%): 571.4 (100) $[M+2H]^{2+}$, 1141.7 (28) $[M+H]^+$; for NMR data see Tables S14–S15 in the Supporting Information.

NMR experiments

The NMR samples contained **3a** or **3b** (5 mM) dissolved in [D_6]DMSO and in [D_3]MeOH and gramicidine S or **4** (20 mM) dissolved in [D_6]DMSO. All spectra were recorded on a Bruker Avance III 600 equipped with a 5 mm quadruple-resonance (^1H, ^{13}C, ^{15}N, ^{31}P). Homonuclear 2D spectra DQF-COSY, TOCSY, and ROESY were typically recorded in the phase-sensitive mode using the States-TPPI method as data matrices of 256–512 real (t_1)×2048 (t_2) complex data points; 8–64 scans per t_1 increment with 1.5 s recovery delay and spectral width of 6009 Hz in both dimensions were used. The mixing times were 80 ms for TOCSY and 300 ms spinlock for ROESY experiments. In addition, 2D heteronuclear spectra ^{15}N-^1H, ^{13}C-^1H HSQC, and ^{13}C-^1H HMBC were acquired to fully assign the oligomers (8–128 scans, 256 real (t_1)×2048 (t_2) complex data points). Spectra were processed and visualized with Topspin 3.0 (Bruker Biospin) on a Linux Station. The matrices were zero-filled to 1024 (t_1)×2048 (t_2) points after apodization by shifted sine-square multiplication and linear prediction in the F1 domain. Chemical shifts were referenced to TMS.

Structure calculations

Parameter files for the ornithine residue were taken from the Amber parameter database provided by the Bryce group at the University of Manchester.[17] The ATC amino acid was built using Sirius,[18] parameter files were then generated using Antechamber and the R.E.D. server.[19] Leap was then used to create the topology and coordinate files for **3a**, **3b** and **4**.

^1H chemical shifts were assigned according to classical procedures. NOE cross-peaks were integrated and assigned within the NMRView software.[20] The volume of a ROE between methylene pair protons was used as a reference of 1.8 Å. The lower bound for all restraints was fixed at 1.8 Å and upper bounds at 2.7, 3.3, and 5.0 Å, for strong, medium, and weak correlations, respectively. Pseudo-atom corrections of the upper bounds were applied for unresolved aromatic, methylene, and methyl protons signals as described previously.[21] Structure calculations were performed with AMBER 10[22] in two stages: cooking and simulated annealing (SA) in vacuum. The cooking stage was performed at 500 K to generate 100 initial random structures. SA calculations were carried during 20 ps (20000 steps, 1 fs long) as described elsewhere. First, the temperature was risen quickly and was maintained at 1000 K for the first 5000 steps, then the system was cooled gradually from 1000 K to 100 K from step 5001 to 18000 and finally the temperature was brought to 0 K during the 2000 remaining steps. For the 3000 first steps, the force constant of the distance restraints was increased gradually from 2.0 kcal mol^{-1} Å to 20 kcal mol^{-1} Å. For the rest of the simulation (step 3001 to 20000), the force constant was kept at 20 kcal mol^{-1} Å. The calculations were launched in vacuum for **3a**, **3b**, and **4**. The 20 lowest energy structures with no violations >0.3 Å were considered as representative of the peptide structure. The representation and quantitative analysis were carried out using Ptraj,[23] MOLMOL,[24] and PyMOL.[25] The 20 lowest energy structures of **3a** and **3b** peptidomimetics were used for a molecular dynamic simulation during 50 ns in a methanol box (see the MD section).

© 2014 Wiley-VCH Verlag GmbH & Co. KGaA, Weinheim

Molecular dynamic simulations in an explicit solvent box

The lowest energy structures of **3a** and **3b** were immersed in a methanol box with a layer of 10 Å for a molecular dynamic simulation stage of 50 ns using the following protocol. First, a minimization procedure consisting in two stages: 1) The solute was kept fixed while the solvent methanol positions are optimized (10000 steps) and then 2) the entire system was minimized (2500 steps). 3) The system was then allowed to heat up from 0 to 300 K at constant volume keeping the solute fixed (50000 steps, that is, 50 ps). 4) The whole system was equilibrated at a constant pressure of 1 atm and at 300 K over 50000 steps (50 ps). 5) Molecular dynamic simulations were finally performed at 300 K and 1 atm during 50 ns (time steps of 0.1 fs). NMR inter-residues restraints were applied during the entire runs (Tables S11 and S12 in the Supporting Information).

DFT calculations

From MD simulations in methanol, compound **3a** underwent a transition after 1.5 ns from a twist-turn structure to a reverse-turn structure stabilized by a bifurcated $C_{9/12}$ pseudocycle. However, the reverse-turn structure did not provide any characteristic NOE correlation probed by NMR experiments. So, the twist-turn and reverse-turn structures were reoptimized at the B3LYP/6–31G(d) level of theory. Then, the single-point energies of this reverse-turn structure and the twist-turn structure obtained from NMR experiments were calculated at the same level of theory with the conductor-like polarizable continuum model (CPCM)[8] in methanol. The twist-turn structure was found to be more stable by 3.40 kcal mol^{-1} than the reverse-turn structure in methanol, which indicates the relative populations of 99.7 and 0.3% for twist- and reverse-turn structures at 298 K, respectively.

The two NMR structures **3a** and **3b** were optimized at the B3LYP/6–31G(d) level of theory. To figure out the relative strength of the C_9 hydrogen bond between the amide hydrogen of the third Ile residue and the carbonyl oxygen of the first Val residue, a natural bond orbital (NBO) analysis was performed for the optimized structures at the B3LYP/6–31+G(d,p) level of theory. The three kinds of properties were compared to understand the relative strength of the hydrogen bond and the calculated results are shown in Table 1. The first values are the natural atomic charges of oxygen (the carbonyl oxygen of the first Val residue) and hydrogen (the amide hydrogen of the third Ile residue). The second value is the Wiberg bond index of the N–H bond of the third Ile residue, which shows the strength of a bond. The third value is the second perturbation energy (ΔE_2) of the lone pair orbitals of the oxygen with the corresponding N–H antibonding orbital, which is called the hyperconjugation due to the charge transfer. We can say that the hydrogen bond is strong when the magnitudes of atomic charges become larger, the Wiberg index becomes smaller, and ΔE_2 becomes larger.

Circular dichroism

Circular dichroism (CD) experiments were carried out using a Jasco J815 spectropolarimeter. The spectra were recorded with of compounds **3a** (0.2 mM), **3b** (0.2 mM) and **4** (0.1 mM) dissolved in MeOH using a 1 mm path length CD cuvette at 20 °C, over a wavelength range of 190–300 nm. Continuous scanning mode was used, with a response of 1.0 s with 0.2 nm steps and a bandwidth of 2 nm. The signal-to-noise ratio was improved by acquiring each spectrum over an average of two scans. The baseline was corrected by subtracting the background from the sample spectrum.

Antimicrobial activities

GS and **4** were dissolved at 1 mg mL^{-1} in DMSO then successively diluted in the same solvent. DMSO was used as negative control. The antibacterial activities of GS and **4** were monitored by liquid growth inhibition assay performed in microtiter plates. Briefly, a DMSO solution (10 μL) of GS or **4** at different concentrations (ranging from 1 mg mL^{-1} to 1 μg mL^{-1}; 100 to 0.1 μg mL^{-1} final concentrations, respectively) was added to a suspension of a mid-logarithmic phase culture of bacteria (90 μL; $OD_{620nm} = 0.02$) in poor-broth nutrient medium. Cultures were carried out in triplicate and microbial growths were assessed by measuring turbidity at 620 nm after incubation (48 h, 37 °C). The MIC was defined as the lowest concentration of antibiotic where bacterial growth was not detected. The MICs were determined from independent triplicate assays and were based on a serial twofold plus or minus system. To be considered valid, MIC determinations for each of the 3 replicates had to be within plus or minus 1 dilution of each other.

Haemolytic activities

GS and **4** (2 mM) were dissolved in DMSO then successively diluted in the same solvent. The haemolytic activities of GS and **4** were monitored in microtiter plates. PBS (45 μL) and sample (5 μL) were added to a freshly prepared blood solution (50 μL; 5×10^5 erythrocytes per μL). The mixtures were incubated to the 37 °C during 30 min. After the incubation period, erythrocytes were separated by centrifugation (300 *g*, 10 °C, 10 min). A 50 μL portion of each supernatant was further transferred to a microwell plate to measure the absorbance at 490 nm into a microplate reader. DMSO was used as negative control while SDS (0.1% final concentration) was used for 100% haemolysis.

Acknowledgements

We thank the IBMM, the Laboratoire de Mesure Physique of Montpellier, the CNRS and the University of Montpellier 1 for financial support.

Keywords: amino acids · gramicidin S · hybrid peptide · thiazoles

[1] a) J. S. Richardson, *Adv. Protein Chem.* **1981**, *34*, 167–339; b) C. M. Wilmot, J. M. Thornton, *J. Mol. Biol.* **1988**, *203*, 221–232; c) G. D. Rose, L. M. Gierasch, J. A. Smith, *Adv. Protein Chem.* **1985**, *37*, 1–109; d) E. Vass, M. Hollosi, F. Besson, R. Buchet, *Chem. Rev.* **2003**, *103*, 1917–1954.

[2] a) M. D. Seo, H. S. Won, J. H. Kim, T. Mishig-Ochir, B. J. Lee, *Molecules* **2012**, *17*, 12276–12286; b) R. M. Epand, H. J. Vogel, *Biochim. Biophys. Acta Biomembr.* **1999**, *1462*, 11–28; c) L. T. Nguyen, E. F. Haney, H. J. Vogel, *Trends Biotechnol.* **2011**, *29*, 464–472.

[3] a) Y. J. Chung, L. A. Christianson, H. E. Stanger, D. R. Powell, S. H. Gellman, *J. Am. Chem. Soc.* **1998**, *120*, 10555–10556; b) D. Seebach, A. K. Beck, D. J. Bierbaum, *Chem. Biodiversity* **2004**, *1*, 1111–1239; c) W. S. Horne, S. H. Gellman, *Acc. Chem. Res.* **2008**, *41*, 1399–1408; d) B. R. Huck, J. D. Fisk, S. H. Gellman, *Org. Lett.* **2000**, *2*, 2607–2610; e) R. S. Roy, P. Balaram, *J. Pept. Res.* **2004**, *63*, 279–289; f) S. Chatterjee, R. S. Roy, P. Balaram, *J. R. Soc. Interface* **2007**, *4*, 587–606; g) K. Basuroy, A. Rajagopal, S. Raghothama, N. Shamala, P. Balaram, *Chem. Asian J.* **2012**, *7*, 1671–1678; h) C. André, B. Legrand, C. Deng, C. Didierjean, G. Pickaert, J. Martinez, M. C. Averlant-Petit, M. Amblard, M. Calmes, *Org. Lett.* **2012**, *14*, 960–963.

[4] a) F. Bouillère, S. Thétiot-Laurent, C. Kouklovsky, V. Alezra, *Amino Acids* **2011**, *41*, 687–707; b) A. Trabocchi, E. G. Occhiato, D. Potenza, A. Guarna, *J. Org. Chem.* **2002**, *67*, 7483–7492; c) S. Aravinda, K. Ananda,

© 2014 Wiley-VCH Verlag GmbH & Co. KGaA, Weinheim

N. Shamala, P. Balaram, *Chem. Eur. J.* **2003**, *9*, 4789 – 4795; d) E. Mann, H. Kessler, *Org. Lett.* **2003**, *5*, 4567 – 4570; e) C. Grison, P. Coutrot, S. Geneve, C. Didierjean, M. Marraud, *J. Org. Chem.* **2005**, *70*, 10753 – 10764; f) A. Sengupta, S. Aravinda, N. Shamala, K. M. Raja, P. Balaram, *Org. Biomol. Chem.* **2006**, *4*, 4214 – 4222; g) P. G. Vasudev, K. Ananda, S. Chatterjee, S. Aravinda, N. Shamala, P. Balaram, *J. Am. Chem. Soc.* **2007**, *129*, 4039 – 4048; h) S. Chatterjee, P. G. Vasudev, K. Ananda, S. Raghothama, N. Shamala, P. Balaram, *J. Org. Chem.* **2008**, *73*, 6595 – 6606; i) S. Chatterjee, P. G. Vasudev, S. Raghothama, C. Ramakrishnan, N. Shamala, P. Balaram, *J. Am. Chem. Soc.* **2009**, *131*, 5956 – 5965; j) S. Thetiot-Laurent, F. Bouillere, J. P. Baltaze, F. Brisset, D. Feytens, C. Kouklovsky, E. Miclet, V. Alezra, *Org. Biomol. Chem.* **2012**, *10*, 9660 – 9663; k) S. K. Maji, R. Banerjee, D. Velmurugan, A. Razak, H. K. Fun, A. Banerjee, *J. Org. Chem.* **2002**, *67*, 633 – 639; l) Y. K. Kang, B. J. Byun, *Biopolymers* **2012**, *97*, 1018 – 1025.

[5] L. Mathieu, B. Legrand, C. Deng, L. Vezenkov, E. Wenger, C. Didierjean, M. Amblard, M. C. Averlant-Petit, N. Masurier, V. Lisowski, J. Martinez, L. T. Maillard, *Angew. Chem.* **2013**, *125*, 6122 – 6126; *Angew. Chem. Int. Ed.* **2013**, *52*, 6006 – 6010.

[6] N. H. Andersen, J. W. Neidigh, S. M. Harris, G. M. Lee, Z. Liu, H. Tong, *J. Am. Chem. Soc.* **1997**, *119*, 8547 – 8561.

[7] a) X. Daura, K. Gademann, H. Schafer, B. Jaun, D. Seebach, W. F. van Gunsteren, *J. Am. Chem. Soc.* **2001**, *123*, 2393 – 2404; b) J. Dolenc, J. H. Missimer, M. O. Steinmetz, W. F. van Gunsteren, *J. Biomol. NMR* **2010**, *47*, 221 – 235; c) J. R. Allison, M. Muller, W. F. van Gunsteren, *Protein Sci.* **2010**, *19*, 2186 – 2195; d) Z. Gattin, A. Glattli, B. Jaun, W. F. van Gunsteren, *Biopolymers* **2007**, *85*, 318 – 332.

[8] V. Barone, M. Cossi, *J. Phys. Chem. A* **1998**, *102*, 1995 – 2001.

[9] Gaussian 03, Revision D.01, M. J. Frisch, G. W. Trucks, H. B. Schlegel, G. E. Scuseria, M. A. Robb, J. R. Cheeseman, J. A. Montgomery Jr., T. Vreven, K. N. Kudin, J. C. Burant, J. M. Millam, S. S. Iyengar, J. Tomasi, V. Barone, B. Mennucci, M. Cossi, G. Scalmani, N. Rega, G. A. Petersson, H. Nakatsuji, M. Hada, M. Ehara, K. Toyota, R. Fukuda, J. Hasegawa, M. Ishida, T. Nakajima, Y. Honda, O. Kitao, H. Nakai, M. Klene, X. Li, J. E. Knox, H. P. Hratchian, J. B. Cross, C. Adamo, J. Jaramillo, R. Gomperts, R. E. Stratmann, O. Yazyev, A. J. Austin, R. Cammi, C. Pomelli, J. W. Ochterski, P. Y. Ayala, K. Morokuma, G. A. Voth, P. Salvador, J. J. Dannenberg, V. G. Zakrzewski, S. Dapprich, A. D. Daniels, M. C. Strain, O. Farkas, D. K. Malick, A. D. Rabuck, K. Raghavachari, J. B. Foresman, J. V. Ortiz, Q. Cui, A. G. Baboul, S. Clifford, J. Cioslowski, B. B. Stefanov, G. Liu, A. Liashenko, P. Piskorz, I. Komaromi, R. L. Martin, D. J. Fox, T. Keith, M. A. Al-Laham, C. Y. Peng, A. Nanayakkara, M. Challacombe, P. M. W. Gill, B. Johnson, W. Chen, M. W. Wong, C. Gonzalez, J. A. Pople, Gaussian, Inc., Wallingford CT, **2004**.

[10] F. Weinhold in *Encyclopedia of Computational Chemistry, Vol. 3* (Eds.: P. v. R. Schleyer, N. L. Allinger, T. Clark, J. Gasteiger, P. A. Kollman, H. F. Schaefer, III, P. R. Schreiner), John Wiley & Sons, Chichester **1998**, pp. 1792 – 1811.

[11] K. B. Wiberg, *Tetrahedron* **1968**, *24*, 1083.

[12] L. H. Kondejewski, S. W. Farmer, D. S. Wishart, R. E. Hancock, R. S. Hodges, *Int. J. Pept. Prot. Res.* **1996**, *47*, 460 – 466.

[13] E. J. Prenner, R. N. Lewis, R. N. McElhaney, *Biochim. Biophys. Acta Biomembr.* **1999**, *1462*, 201 – 221.

[14] a) D. C. Hodgkin, B. M. Oughton, *Biochem. J.* **1957**, *65*, 752 – 756; b) M. Doi, S. Fujita, Y. Katsuya, M. Sasaki, T. Taniguchi, H. Hasegawa, *Arch. Biochem. Biophys.* **2001**, *395*, 85 – 93; c) K. Yamada, M. Unno, K. Kobayashi, H. Oku, H. Yamamura, S. Araki, H. Matsumoto, R. Katakai, M. Kawai, *J. Am. Chem. Soc.* **2002**, *124*, 12684 – 12688; d) M. Kawai, H. Yamamura, R. Tanaka, H. Umemoto, C. Ohmizo, S. Higuchi, T. Katsu, *J. Peptide Res.* **2005**, *65*, 98 – 104; e) C. Solanas, B. G. de La Torre, M. Fernandez-Reyes, C. M. Santiveri, M. A. Jimenez, L. Rivas, A. I. Jimenez, D. Andreu, C. Cativiela, *J. Med. Chem.* **2010**, *53*, 4119 – 4129; f) M. Tamaki, K. Takanashi, T. Harada, K. Fujinuma, M. Shindo, M. Kimura, Y. Uchida, *Chem. Pharm. Bull.* **2011**, *59*, 1481 – 1484; g) M. van der Knaap, L. T. Lageveen, H. J. Busscher, R. Mars-Groenendijk, D. Noort, J. M. Otero, A. L. Llamas-Saiz, M. J. van Raaij, G. A. van der Marel, H. S. Overkleeft, M. Overhand, *ChemMedChem* **2011**, *6*, 840 – 847; h) J. Xiao, B. Weisblum, P. Wipf, *Org. Lett.* **2006**, *8*, 4731 – 4734; i) E. Kamysz, B. Mickiewicz, W. Kamysz, S. Bielinska, S. Rodziewicz-Motowidlo, J. Ciarkowski, *J. Pept. Sci.* **2011**, *17*, 211 – 217; j) V. V. Kapoerchan, E. Spalburg, A. J. de Neeling, R. H. Mars-Groenendijk, D. Noort, J. M. Otero, P. Ferraces-Casais, A. L. Llamas-Saiz, M. J. van Raaij, J. van Doorn, G. A. van der Marel, H. S. Overkleeft, M. Overhand, *Chem. Eur. J.* **2010**, *16*, 4259 – 4265; k) G. M. Grotenbreg, A. E. Buizert, A. L. Llamas-Saiz, E. Spalburg, P. A. van Hooft, A. J. de Neeling, D. Noort, M. J. van Raaij, G. A. van der Marel, H. S. Overkleeft, M. Overhand, *J. Am. Chem. Soc.* **2006**, *128*, 7559 – 7565.

[15] A. L. Llamas-Saiz, G. M. Grotenbreg, M. Overhand, M. J. van Raaij, *Acta Crystallogr. Sect. D* **2007**, *63*, 401 – 407.

[16] a) L. H. Kondejewski, M. Jelokhani-Niaraki, S. W. Farmer, B. Lix, C. M. Kay, B. D. Sykes, R. E. Hancock, R. S. Hodges, *J. Biol. Chem.* **1999**, *274*, 13181 – 13192; b) C. McInnes, L. H. Kondejewski, R. S. Hodges, B. D. Sykes, *J. Biol. Chem.* **2000**, *275*, 14287 – 14294.

[17] http://www.pharmacy.manchester.ac.uk/bryce/amber/.

[18] http://www.ngbw.org/sirius/.

[19] E. Vanquelef, S. Simon, G. Marquant, E. Garcia, G. Klimerak, J. C. Delepine, P. Cieplak, F.-Y. Dupradeau, *Nucl. Acids Res.* **2011**, *39*, W511 – W517.

[20] B. A. Johnson, R. A. Blevins, *J. Biomol. NMR* **1994**, *4*, 603 – 614.

[21] K. Wüthrich, *NMR of Proteins and Nucleic Acids*, Wiley-Interscience, New York, **1986**.

[22] AMBER 10, D. A. Case, T. A. Darden, T. E. Cheatham, III, C L. Simmerling, J. Wang, R. E. Duke, R. Luo, M. Crowley, R. C. Walker, W. Zhang, K. M. Merz, B. Wang, S. Hayik, A. Roitberg, G. Seabra, I. Kolossvary, K. F. Wong, F. Paesani, J. Vanicek, X. Wu, S. R. Brozell, T. Steinbrecher, H. Gohlke, L. Yang, C. Tan, J. Mongan, V. Hornak, G. Cui, D. H. Mathews, M. G. Seetin, C. Sagui, V. Babin, P. A. Kollman, University of California, San Francisco, **2008**.

[23] D. R. Roe and T.E. Cheatham, *J. Chem. Theory Comput.*, **2013**, *9*, 3084 – 3095.

[24] R. Koradi, M. Billeter, K. Wuthrich, *J. Mol. Graph.* **1996**, *14*, 51 – 55.

[25] Delano Scientific, http://www.pymol.org/

Received: February 14, 2014
Published online on March 25, 2014

© 2014 Wiley-VCH Verlag GmbH & Co. KGaA, Weinheim